Journal of Power Sources 196 (2011) 3178–3185

Contents lists available at ScienceDirect

Journal of Power Sources

journal homepage: www.elsevier.com/locate/jpowsour

Percolation micro-model to predict the effective properties of the composite electrode with poly-dispersed particle sizes

Daifen Chen [a,*], Liu Lu [b], Jiayu Li [b], Zidong Yu [a], Wei Kong [b], Huayang Zhu [c]

[a] School of Naval Architecture and Ocean Engineering, Jiangsu University of Science and Technology, Zhenjiang 212003, China
[b] Department of Physics, University of Science and Technology of China, Hefei 230026, China
[c] Engineering Division, Colorado School of Mines, Golden, CO 80401, USA

ARTICLE INFO

Article history:
Received 22 September 2010
Received in revised form
19 November 2010
Accepted 22 November 2010
Available online 27 November 2010

Keywords:
Solid oxide fuel cell
Composite electrode
Coordination number
Percolation theory
Inter-particle conductivity
Triple phase boundary

ABSTRACT

A percolation micro-model is developed to predict the effective properties of the composite electrode consisting of poly-dispersed electronic and ionic-conducting particles. The analytical expressions for the percolated triple-phase-boundary (TPB) lengths, hydraulic pore radius and intra/inter-particle conductivities have been formed. The model shows that the percolated TPB lengths of a composite electrode consisting of poly-dispersed particle sizes for both materials (i.e., having a normal distribution with a non-dimensional standard deviation of 0.4) are about 32% lower than that of the composite electrode with mono-sized particles. And the higher percolated TPB lengths can be achieved by reducing the mean particle size of each material and narrowing the particle size distribution. A composite cathode may benefit from it, because of its low electrochemical activity. The model also shows that the composite electrode with large mean particle size radii ratio between the electrode- and electrolyte-materials and broad particle size distributions can not only provide higher inter-particle ion conductivity, but also reduce the percolation volume fraction threshold of the electrode-material. And this may be helpful for a composite anode to obtain a higher overall ion conductivity.

1. Introduction

The application of a composite electrode with both electronic and ionic conducting materials has been regarded as an attractive alterative compared to the electrode with single material by extending the electrochemical reaction zone from the dense electrolyte into the composite electrode [1–4]. This in turn may significantly increase the solid-oxide-fuel-cell (SOFC) performance [5–8]. A typical porous composite electrode is a mixture of the electronic conducting materials (i.e., lanthanum-doped strontium manganate (LSM) for cathode and Ni for anode) and ionic conducting materials (i.e., yttria-stabilized zirconia (YSZ)) [3,5]. And a proper SOFC composite electrode may have, but is not limited to, the following characteristics: (i) a proper thermal conductivity that matches the other components, (ii) a sufficient mechanical strength to support the cell, (iii) a percolated porous path for the reaction species to transport from the channel into the reaction sites. The 'percolated' in here is defined as the contiguous connection through the whole electrode structure, (iv) a percolated electronic conducting path (through Ni or LSM) for the electrons to conduct from the reaction spots to the current collector, (v) a percolated ionic conducting path (through YSZ) for the ions to propagate from the dense electrolyte to the reaction spots, (vi) the percolated triple-phase-boundaries (TPBs) to support the electrochemical reaction. As the electrochemical reaction refers to electrons, ions and reaction species, it can only occur at the TPBs, where the electronic conducting, ionic conducting and porous phases coexist (i.e., Ni-YSZ-pore) and each phase belong to a percolated network, respectively. These TPBs are defined as the percolated TPBs [9]. These percolated TPBs, however, are only potential electrochemical active. How much part of them can be active again rely on the composite electrode properties and the thickness of the composite electrode [4]. Conclusively, the SOFC performance is significantly affected by the composite electrode properties. This in turn relies on the particular microstructure of the composite electrode. As the fabrication technology of a composite electrode becomes sophisticated, the understanding of the detailed knowledge of microstructure and its effect on the electrode properties are receiving considerable attentions [5,10–13].

In the past decades, parametric studies for the composite electrodes have been widely made by many researchers through experiments [10,11,14–16], random packing reconstruction methods [17–20] and percolation micro-models [7,9,21–24]. (i) The experimental methods rely primarily on the stereological meth-

* Corresponding author. Tel.: +86 511 84417398; fax: +86 511 84404433.
E-mail address: dfchen@mail.ustc.edu.cn (D. Chen).

0378-7753/$ – see front matter © 2010 Elsevier B.V. All rights reserved.
doi:10.1016/j.jpowsour.2010.11.107

ods [10,25–27]. Recently, the focused ion-beam scanning electron microscopy has been attempted to obtain the high resolution 3D image of a composite electrode [10,11,14,28–29]. All of them greatly enhance the understanding of the composite electrode microstructure and are helpful for developing the theory model in relating the microstructure and the electrode properties. Certainly, the theory approaches are also necessary, because the experimental methods are still expensive and time consuming, and require the use of the hard-to-access facilities (i.e., focused ion-beam, synchrotron radiation facilities and laser scanning confocal microscopy) [10,11,14,30]. (ii) The random packing reconstruction methods are mainly based on the random packing of sphere particles, in which a composite electrode is considered as a porous structure formed of randomly distributed sphere particles. Ali et al. [19], Schneider et al. [18], and Golbert et al. [17] have reconstructed the binary composite structures with mono size particles for each material to evaluate the percolated TPB lengths. Recently, Kenney et al. [20] have further extended the model and reconstructed a binary composite structure with poly-disperse particles to predict the effective electrode properties. However, only limited properties have been calculated, the prediction of some other electrode properties such as the hydraulic pore radius, intra/inter-particle conductivities and so on have not yet been achieved by the random packing reconstruction methods as far as we know. And it is difficult to incorporate the reconstructed structures into the cell-level models for simultaneously exploring the effects of various microstructure parameters on the SOFC performance. (iii) The percolation micro-models use the percolation theory and coordination number theory to represent the microstructure of a composite electrode developed by the random packing reconstruction methods. And analytical expressions are derived to relate the electrode properties and the microstructure parameters [22,31]. Therefore, the percolation micro-model can be considered as an extension of the random packing reconstruction method, and is sufficiently accurate enough in predicting the electrode properties from the microstructure parameters [22,24]. It is also convenient in coupling with the cell-level models [4]. Bouvard et al. [32] and Suzuki et al. [31] have developed the micro-models to represent the microstructure of a binary random packing sphere structure. And the percolation micro-models have been further developed by Costamagna et al. [22], Chan et al. [21] and Janardhanan et al. [24] to relate the composite electrode microstructure and the effective properties. Recently, Chen et al. [9] have generalized the percolation micro-model of a binary random packed system to a model of 3-component random packed system for predicting the effective properties of a composite electrode with LSM particles, coarse and fine YSZ particles. More recently, the percolation micro-models have been further incorporated into the cell-level models to evaluate the effects of electrode microstructure parameters on the SOFC performance [7,8,23].

In the early work, each material phase of the composite electrode was limited to the mono-sized particles. But, the SOFC composite ceramic electrodes are typically poly-disperse powders that each material may have a broad particle size distribution, and this can have significant impacts on the effective electrode properties. In this paper, a percolation micro-model is developed to predict the effective properties of the composite electrodes with a distributed particle sizes that match the actual ceramic powders. Analytical expressions are derived to predict the percolated TPB lengths, intra/inter-particle conductivities, etc. based on the microstructure parameters. The percolation micro-model is validated through comparing with the random packing reconstruction method. Furthermore, all the effective properties are represented in non-dimensional form for providing generality in practical applications. And the percolation micro-model is particularly focused on the applications in optimizing the SOFC cathodes and anodes, respectively.

2. Theory and method

2.1. Percolation micro-model for the composite electrodes with multiple particle sizes

2.1.1. Coordination number and microstructure parameters

Consider a multi-component mixture of randomly packed spherical particles with M type particle sizes. The average number of contacts Z_k between k-type particles and all neighboring particles is [9],

$$Z_k = \sum_{\ell=1}^{M} Z_{k,\ell}, \tag{1}$$

where $Z_{k,\ell}$ is the number of contacts between a k-particle and all the neighboring ℓ-particles. It can be estimated as [9],

$$Z_{k,\ell} = 0.5\left(1 + \frac{r_k^2}{r_\ell^2}\right)\bar{Z}\frac{\psi_\ell/r_\ell}{\sum_{k=1}^{M}\psi_k/r_k}, \tag{2}$$

where r_k is the radius of k-particle. $\bar{Z}$ is the average coordination number of all particles, which is widely assumed to be 6 [21,22,33,34]. ψ_k is the volume fraction of all k-particles.

2.1.2. Effective electrode properties and coordination number

A porous composite electrode is usually assumed to have two type materials: the ionic-conducting electrolyte-phase material (labeled as 'el' such as YSZ) and electronic-conducting electrode-phase material (labeled as 'ed' such as Ni or LSM). Due to the ceramic powders are typically poly-disperse powders, a composite electrode consisting of m type particle sizes for the electronic-conducting material (designated as ed_1, ed_2, …, ed_m) and n type particle sizes for the ionic-conducting material (designated as el_1, el_2, …, el_n) is initially considered in here ($m+n=M$).

Denoting ψ_{ed_k} and ψ_{el_k} as the volume fraction of ed_k- and el_k-particles, respectively. The total volume fractions of the electronic-conducting and ionic-conducting materials can be estimated as,

$$\psi_{\mathrm{ed}} = \sum_{k=1}^{m}\psi_{\mathrm{ed}_k}, \qquad \psi_{\mathrm{el}} = \sum_{k=1}^{n}\psi_{\mathrm{el}_k}. \tag{3}$$

And the relative volume fraction of each type particle sizes within the electronic-conducting and ionic-conducting materials can be represented as

$$\psi^0_{\mathrm{ed}_k} = \frac{\psi_{\mathrm{ed}_k}}{\psi_{\mathrm{ed}}}, \qquad \psi^0_{\mathrm{el}_k} = \frac{\psi_{\mathrm{el}_k}}{\psi_{\mathrm{el}}}. \tag{4}$$

The percolated TPB lengths per unit volume ($\lambda^V_{\mathrm{TPB,per}}$) is proportional to the contact perimeter between ed_k-particle and el_ℓ-particle ($l_{\mathrm{ed}_k,\mathrm{el}_\ell}$), the number of contact points per unit volume, which is the product of the numbers of ed_k-particles per unit volume ($n^V_{\mathrm{ed}_k}$) and their coordination numbers with other el-particles ($Z_{\mathrm{ed}_k,\mathrm{el}_\ell}$), and the probabilities of ed_k- and el_ℓ-particles belonging to the percolated clusters (P_{ed_k} and P_{el_ℓ}),

$$\lambda^V_{\mathrm{TPB,per}} = \sum_{k=1}^{m}\sum_{\ell=1}^{n} l_{\mathrm{ed}_k,\mathrm{el}_\ell} n^V_{\mathrm{ed}_k} Z_{\mathrm{ed}_k,\mathrm{el}_\ell} P_{\mathrm{ed}_k} P_{\mathrm{el}_\ell}. \tag{5}$$

As indicated in Fig. 1, the contact perimeter ($l_{\mathrm{ed}_k,\mathrm{el}_\ell}$) can be estimated as $l_{\mathrm{ed}_k,\mathrm{el}_\ell} = 2\pi\ \min(r_{\mathrm{ed}_k}, r_{\mathrm{el}_\ell})\sin\theta$, where r_{ed_k} and r_{el_ℓ} are the radii of ed_k-particles and el_ℓ-particles, θ is the contact angle.

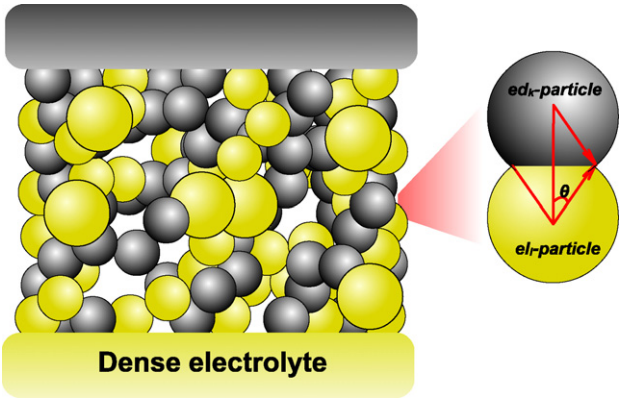

Fig. 1. Illustration of a composite electrode with both coarse and fine electrolyte-particle sizes. And the overlapping between ed$_k$-particle and el$_\ell$-particle is described on the right side.

The number of ed$_k$-particles per unit volume within the entire composite electrode structure can be estimated as [7,22],

$$n^V_{\mathrm{ed}_k} = \frac{(1-\phi_g)\psi_{\mathrm{ed}_k}}{4\pi r^3_{\mathrm{ed}_k}/3}, \tag{6}$$

where ϕ_g is the porosity.

Since only the percolated TPBs are potential electrochemical active, it is the percolation probability to account for the effects of the percolated TPB lengths. For a binary mixture with two mono sized particles, ed$_1$- and el$_1$-particles, the percolation probability of el$_1$-particles can be estimated as $P_{\mathrm{el}_1} = [1-((3.764-Z_{\mathrm{el}_1,\mathrm{el}_1})/2)^{2.5}]^{0.4}$ [22].

However, for a composite electrode with n type particle sizes of electrolyte-material as indicated in Fig. 1, the percolation probability of el$_k$-particles belonging to the percolated clusters depends not only upon the coordination numbers among the same size of electrolyte-particles ($Z_{\mathrm{el}_k,\mathrm{el}_k}$), but also on the mutual coordination numbers among the similar materials ($Z_{\mathrm{el}_k,\mathrm{el}_\ell}$ $(k\neq\ell)$). In order to calculate the percolation probability of el$_k$-particles, the average number of contacts between el$_k$-particles and all the neighboring electrolyte-particles ($Z_{\mathrm{el}_k,\mathrm{el}} = \sum_{\ell=1}^{n} Z_{\mathrm{el}_k,\mathrm{el}_\ell}$) is used here,

$$P_{\mathrm{el}_k} = \left[1-\left(\frac{3.764-\sum_{\ell=1}^{n} Z_{\mathrm{el}_k,\mathrm{el}_\ell}}{2}\right)^{2.5}\right]^{0.4}. \tag{7}$$

This expression is validated by comparing the calculated results through the percolation micro-model with the results reported by Kenney et al. [20]. Similarly, the percolation probability of ed$_k$-particles can also be estimated using the average number of contacts between ed$_k$-particles and all the neighboring electrode-particles ($Z_{\mathrm{ed}_k,\mathrm{ed}}$).

The electrochemical reaction not only takes place within the composite electrode, but also at the interface of the composite electrode and dense electrolyte [7]. And the percolated TPB lengths per unit electrolyte surface area can be estimated as,

$$\lambda^S_{\mathrm{TPB,per}} = \sum_{k=1}^{m} (2\pi r_{\mathrm{ed}_k}\sin\theta) n^S_{\mathrm{ed}_k} P_{\mathrm{ed}_k}, \tag{8}$$

where the number of ed$_k$-particles per unit dense electrolyte surface is $n^S_{\mathrm{ed}_k} = (1-\phi_g)\psi_{\mathrm{ed}_k} 2\pi r^2_{\mathrm{ed}_k}/3$ [7,9].

The effective intra-particle ion conductivity based on the geometric dimensions ($\sigma^{\mathrm{tra,eff}}_{\mathrm{el}}$) is primarily determined by the effective relative density of the percolated electrolyte-particles (ξ_{el}) [35]. Jeon et al. [7] proposed that the intra-particle conductivity can be estimated as,

$$\frac{\sigma^{\mathrm{tra,eff}}_{\mathrm{el}}}{\sigma^{\mathrm{tra},0}_{\mathrm{el}}} = \xi^{\mu}_{\mathrm{el}} = \left[\sum_{k=1}^{n}\left(1-\phi_g\right)\psi_{\mathrm{el}_k} P_{\mathrm{el}_k}\right]^{\mu}, \tag{9}$$

where $\sigma^{\mathrm{tra},0}_{\mathrm{el}}$ is the intrinsic ion conductivity. The Bruggeman factor (μ) is used to include the effects of tortuous conduction phases. Similar expression can also be applied to calculate the effective intra-particle electron conductivity of the composite electrode.

For a electronic-conducting electrode-phase within the composite electrode, the resistance due to the inter-particle conductivity is usually negligibly small [9]. However, the inter-particle ion conductivity can play an important role on the overall ionic conductivity for a ceramic material (i.e., YSZ), especially at intermediate and low temperatures [9,35]. And the particle size, inter-particle area, doping level and inter-particle interface thickness can significantly affect the inter-particle ion conductivity. The inter-particle ion conductivity ($\sigma^{\mathrm{ter,eff}}_{\mathrm{el}}$) may be evaluated as [9,21],

$$\frac{\sigma^{\mathrm{ter,eff}}_{\mathrm{el}}}{\sigma^{\mathrm{ter},0}_{\mathrm{el}}} = \frac{\sum_{k=1}^{n}\sum_{\ell=1}^{n} 2a_{\mathrm{el}_k,\mathrm{el}_\ell}(r_{\mathrm{el}_k})^2 n^V_{\mathrm{el}_k} Z_{\mathrm{el}_k,\mathrm{el}_\ell} P_{\mathrm{el}_k}}{\delta}, \tag{10}$$

where $\sigma^{\mathrm{ter},0}_{\mathrm{el}}$ is the intrinsic ionic conductivity of the inter-particle interface. $a_{\mathrm{el}_k,\mathrm{el}_\ell} = \pi(\min(r_{\mathrm{el}_k}, r_{\mathrm{el}_\ell})\sin\theta)^2$ is the surface area per contact between two electrolyte-particles. δ is the thickness of the inter-particle interface.

The hydraulic radius is used mainly for describing the flow in a non-circular tube, and is also an essential parameter in modeling the multi-component porous media gas transport using a Dusty–Gas model [36–38]. It can be calculated as [9],

$$r_g = \frac{2}{3}\left(\frac{\phi_g}{x(1-\phi_g)}\right)\left(\sum_{k=1}^{m}\frac{\psi_{\mathrm{ed}_k}}{r_{\mathrm{ed}_k}} + \sum_{\ell=1}^{n}\frac{\psi_{\mathrm{el}_\ell}}{r_{\mathrm{el}_\ell}}\right)^{-1}, \tag{11}$$

where x is an adjustable factor that represents the fraction of solid surface areas belonging to the solid-pore binary phase boundary areas [9].

2.2. Percolation micro-model for the uneven distributed particle sizes

Actually, for a practical composite electrode, the particle sizes for both the ionic-conducting and electronic-conducting materials may have uneven probability distributions. In present paper, the normal distributions are used to represent the particle size distributions of both electronic-conducting and ionic-conducting materials. Certainly, many different kinds of probability distributions can also be applied through the similar approach.

For a particular material, the probability density function of a normal distribution with a specified mean radius ($\bar{r}$) and standard deviation (σ) is given as,

$$f = \frac{1}{\sigma\sqrt{2\pi}}\exp\left(\frac{-(r-\bar{r})^2}{2\sigma^2}\right). \tag{12}$$

And the probability of particle sizes locating in the range of r_1 to r_2 can be calculated as,

$$p = \int_{r_1}^{r_2} f(r)\,dr = \frac{1}{\sigma\sqrt{2\pi}}\int_{r_1}^{r_2}\exp\left(\frac{-(r-\bar{r})^2}{2\sigma^2}\right)dr. \tag{13}$$

To provide considerable generality in practical application, Eq. (13) is rewritten as a function of the non-dimensional radius ($r/\bar{r}$) as,

$$p = \int_{r_1/\bar{r}}^{r_2/\bar{r}} f'\left(\frac{r}{\bar{r}}\right)d\frac{r}{\bar{r}} = \frac{1}{\sigma'\sqrt{2\pi}}\int_{r_1/\bar{r}}^{r_2/\bar{r}}\exp\left(\frac{-(r/\bar{r}-1)^2}{2\sigma'^2}\right)d\frac{r}{\bar{r}}, \tag{14}$$

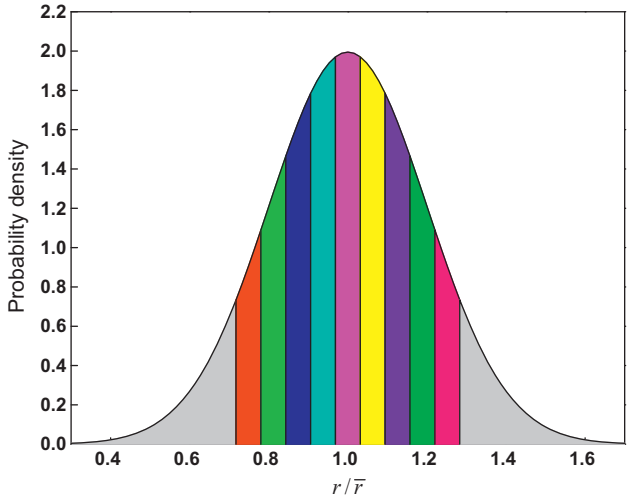

Fig. 2. The probability density of a normal distribution as a function of $r/\bar{r}$ with $\sigma' = 0.2$. The range $(-\sqrt{2}\sigma' + 1, \quad \sqrt{2}\sigma' + 1)$ is discretized into 9 type particle sizes to represent the particle size distribution of each material.

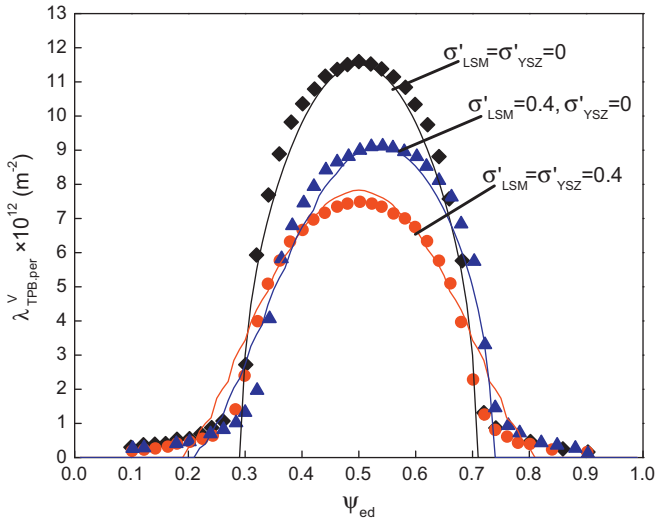

Fig. 3. Comparison between the percolation micro-model results (lines) and the results based on the random packing reconstruction method (points) [20]. $\lambda^{V}_{TPB,per}$ as functions of ψ_{ed}, σ'_{ed} and σ'_{el} with $\bar{r}_{ed} = \bar{r}_{el} = 0.25$ μm, $\theta = 29.5^\circ$ and $\phi_g = 30\%$.

where $\sigma' = \sigma/\bar{r}$ is defined as the non-dimensional standard deviation. In this way, the probability density of a normal distribution as a function of $r/\bar{r}$ with $\sigma' = 0.2$ is shown in Fig. 2.

As illustrated in Fig. 2, when a normal distribution is used to represent the particle size distribution of each material, there is continuous particle size distribution. In here, only the range from $-\sqrt{2}\sigma' + 1$ to $\sqrt{2}\sigma' + 1$ is considered, because of $f'(-\sqrt{2}\sigma' + 1) = f'(\sqrt{2}\sigma' + 1) = (1/e)f'(1)$. And the range is discretized into 9 sections, therefore, the particle size distribution of each material is divided into 9 type particle sizes with a step $2\sqrt{2}\sigma'/9$.

In this case, the probability of each type particle size (p_k) can be estimated through Eq. (14). However, it is necessary to mention that the cumulative probability density of all 9 type particle sizes is less than 1, therefore, the probability of each type particle sizes should be normalized as $p_k / \sum_{\ell=1}^{9} p_\ell$. In Table 1, the non-dimensional radii of all 9 type particle sizes and their normalized probabilities are estimated.

And the relative volume fraction of each type particle sizes can be estimated as,

$$\psi_k^0 = \frac{p_k r_k^3}{\sum_{\ell=1}^{9} p_\ell r_\ell^3}. \tag{15}$$

Using the percolation micro-model described above, the effective properties of a composite electrode with the normal particle size distributions can be predicted conveniently. There are only two parameters needed to specific the normal distribution function of each material's particle sizes: the mean particle radius ($\bar{r}$) and the standard deviation (σ) (or the non-dimensional standard deviation ($\sigma' = \sigma/\bar{r}$).

3. Results and discussion

3.1. Model validation

Fig. 3 illustrates the percolated TPB lengths per unit volume ($\lambda^{V}_{TPB,per}$) as a function of the volume fraction of the electrode-material (ψ_{ed}) and the non-dimensional standard deviations of the electrode- and electrolyte-materials (σ'_{ed} and σ'_{el}) with $\bar{r}_{ed} = \bar{r}_{el} = 0.25$ μm, $\theta = 29.5^\circ$ and $\phi_g = 30\%$. As shown in this figure, good agreement is achieved between the results (lines) based on the percolation micro-model and the results (points) based on the random packing reconstruction method reported by Kenney et al. [20]. It demonstrates the suitability of the proposed percolation micro-model in relating the composite electrode properties and the microstructure parameters. It should be pointed out that there exist several transitions in the curves for poly-disperse case (i.e., $\sigma'_{ed} = \sigma'_{el} = 0.4$ or $\sigma'_{ed} = 0.4$, $\sigma'_{el} = 0$). The reason is that the particle size distribution of each material is represented by 9 type particle sizes and each type of particle size may have a different percolation volume fraction threshold according to Eq. (7). Therefore, each type of particle size may cause a small transition in the curve. These transitions can be eliminated by using more types of particle sizes to represent the particle size distribution.

3.2. Percolated TPB lengths

To provide a considerable generality of the percolation micro-model in practical application, all the composite electrode properties are presented in non-dimensional form basing on the underpinning functions. In this way, the results are not specific to a particular composite electrode structure, and once the physical parameters are given, the relevant effective properties can be easily extracted.

Substituting the contact perimeter and particle number loading into Eq. (5), the percolated TPB lengths per unit volume can be rewritten as,

$$\lambda^{V}_{TPB,per} = \sum_{k=1}^{9}\sum_{\ell=1}^{9} \frac{3}{2} \frac{\min(r_{ed_k}, r_{el_\ell})}{r^3_{ed_k}} (1 - \phi_g) \sin\theta \psi_{ed_k} Z_{ed_k, el_\ell} P_{ed_k} P_{el_\ell}. \tag{16}$$

It shows that $\lambda^{V}_{TPB,per}$ depends upon Z_{ed_k, el_ℓ}, P_{ed_k} and P_{el_ℓ}, which are functions of the volume fraction of electrode-material (ψ_{ed}), mean particle radii ratio of the electrode- and electrolyte-materials ($\bar{r}_{el}/\bar{r}_{ed}$) and non-dimensional standard deviations (σ'_{ed} and σ'_{el}).

The non-dimensional form of $\lambda^{V}_{TPB,per}$ can be written as,

$$\tilde{\lambda}^{V}_{TPB,per} = \frac{\lambda^{V}_{TPB,per}}{(1 - \phi_g)\sin\theta/\bar{r}^2_{ed}}. \tag{17}$$

Here, the non-dimensional percolated TPB lengths per unit volume ($\tilde{\lambda}^{V}_{TPB,per}$) is independent of the particular particle radii ($\bar{r}_{ed}$ and $\bar{r}_{el}$), contact angle (θ) and porosity (ϕ_g). However, it doses depend upon the non-dimensional standard deviations (σ'_{ed} and σ'_{el}), volume fraction of the electrode-material (ψ_{ed}) and mean particle radii ratio ($\bar{r}_{el}/\bar{r}_{ed}$).

Table 1
The non-dimensional radii of 9 type particle sizes and their normalized probabilities.

	1	2	3	4	5	6	7	8	9
$r/\bar{r}$	$1-\frac{8\sqrt{2}\sigma'}{9}$	$1-\frac{6\sqrt{2}\sigma'}{9}$	$1-\frac{4\sqrt{2}\sigma'}{9}$	$1-\frac{2\sqrt{2}\sigma'}{9}$	1	$1+\frac{2\sqrt{2}\sigma'}{9}$	$1+\frac{4\sqrt{2}\sigma'}{9}$	$1+\frac{6\sqrt{2}\sigma'}{9}$	$1+\frac{8\sqrt{2}\sigma'}{9}$
p	6.77%	9.53%	12.2%	14.1%	14.8%	14.1%	12.2%	9.53%	6.77%

Fig. 4 shows how $\tilde{\lambda}^{V}_{\mathrm{TPB,per}}$ depends upon ψ_{ed}, σ'_{ed} and σ'_{el} with $\bar{r}_{\mathrm{el}}/\bar{r}_{\mathrm{ed}}=1$. As indicated in Fig. 4, the maximum $\tilde{\lambda}^{V}_{\mathrm{TPB,per}}$ may significantly decrease with the increasing of the non-dimensional standard deviation of each material (σ'_{ed} and σ'_{el}), which represents the particle size distribution of each material. For example, $\tilde{\lambda}^{V}_{\mathrm{TPB,per}}$ with the particle size distributions of $\sigma'_{\mathrm{ed}}=\sigma'_{\mathrm{el}}=0.4$ and $\sigma'_{\mathrm{ed}}=\sigma'_{\mathrm{el}}=0.6$ are 32% and 48% lower than $\tilde{\lambda}^{V}_{\mathrm{TPB,per}}$ with mono particle size distributions ($\sigma'_{\mathrm{ed}}=\sigma'_{\mathrm{el}}=0$) with the same mean particle radii and $\psi_{\mathrm{ed}}=0.5$, respectively. Similarly, the maximal $\tilde{\lambda}^{V}_{\mathrm{TPB,per}}$ with $\sigma'_{\mathrm{ed}}=0.4$, $\sigma'_{\mathrm{el}}=0$ is 21% smaller compared to the maximal $\tilde{\lambda}^{V}_{\mathrm{TPB,per}}$ with $\sigma'_{\mathrm{ed}}=\sigma'_{\mathrm{el}}=0$.

It is important to note that for a composite electrode with $\bar{r}_{\mathrm{ed}}=\bar{r}_{\mathrm{el}}$ and $\sigma'_{\mathrm{ed}}=\sigma'_{\mathrm{el}}$, the volume fraction of the electrode-material (ψ_{ed}) for the maximum $\tilde{\lambda}^{V}_{\mathrm{TPB,per}}$ will be 0.5. For the case $\bar{r}_{\mathrm{ed}}=\bar{r}_{\mathrm{el}}$ but $\sigma'_{\mathrm{ed}}\neq\sigma'_{\mathrm{el}}$, however, ψ_{ed} for the maximum $\tilde{\lambda}^{V}_{\mathrm{TPB,per}}$ may shift. ψ_{ed} for the maximum $\tilde{\lambda}^{V}_{\mathrm{TPB,per}}$ will shift from 0.5 to a higher value for $\sigma'_{\mathrm{ed}}>\sigma'_{\mathrm{el}}$. And ψ_{ed} for the maximum $\tilde{\lambda}^{V}_{\mathrm{TPB,per}}$ will shift from 0.5 to a lower value for $\sigma'_{\mathrm{ed}}<\sigma'_{\mathrm{el}}$.

It is widely agreed that there is a threshold in the volume fraction of the electrode- or electrolyte-material, percolated threshold ($\psi^{\mathrm{t}}_{\mathrm{ed}}$ or $\psi^{\mathrm{t}}_{\mathrm{el}}$), above which the particles form a continuous network through the whole structure [22]. Thus the volume fraction of the electrode-material should be chosen within the range ($\psi^{\mathrm{t}}_{\mathrm{ed}}<\psi_{\mathrm{ed}}<1-\psi^{\mathrm{t}}_{\mathrm{el}}$). In this case, both the electrode- and electrolyte-materials form the connected networks through the entire composite electrode structure. This phenomenon is supported by the shapes of the curves shown in Fig. 4. There are volume fraction thresholds for both the electrode- and electrolyte-materials, below or above the thresholds ($\psi^{\mathrm{t}}_{\mathrm{ed}}$ and $1-\psi^{\mathrm{t}}_{\mathrm{el}}$) there are no percolated TPB lengths. And it can also be found that the increasing of the non-dimensional standard deviations will extend the range of the volume fraction thresholds ($\psi^{\mathrm{t}}_{\mathrm{ed}}\sim(1-\psi^{\mathrm{t}}_{\mathrm{el}})$). For example, the range of $\psi^{\mathrm{t}}_{\mathrm{ed}}\sim(1-\psi^{\mathrm{t}}_{\mathrm{el}})$ may extend from (0.3–0.7) for ($\sigma'_{\mathrm{ed}}=\sigma'_{\mathrm{el}}=0$) to (0.2–0.8) for $\sigma'_{\mathrm{ed}}=\sigma'_{\mathrm{el}}=0.4$.

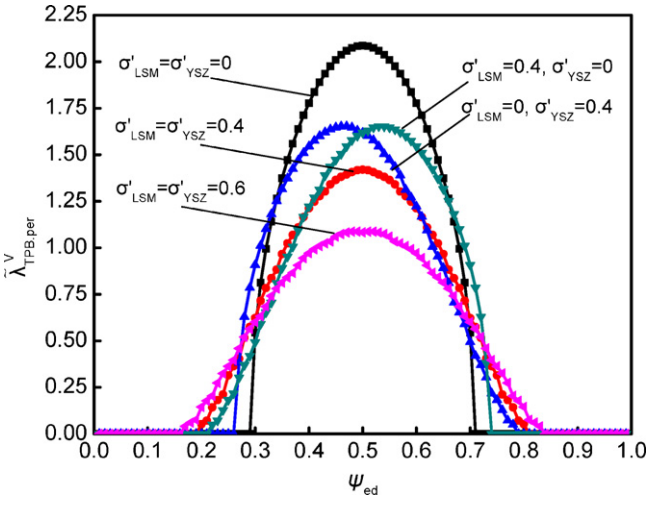

Fig. 4. The effects of ψ_{ed} and non-dimensional standard deviations (σ'_{ed} and σ'_{el}) on $\tilde{\lambda}^{V}_{\mathrm{TPB,per}}$ with $\bar{r}_{\mathrm{el}}/\bar{r}_{\mathrm{ed}}=1$.

Fig. 5 illustrates how $\tilde{\lambda}^{V}_{\mathrm{TPB,per}}$ depends upon ψ_{ed} and $\bar{r}_{\mathrm{el}}/\bar{r}_{\mathrm{ed}}$ with $\sigma'_{\mathrm{ed}}=\sigma'_{\mathrm{el}}=0$ and $\sigma'_{\mathrm{ed}}=\sigma'_{\mathrm{el}}=0.4$, respectively. As indicated in Fig. 5, ψ_{ed} for the maximum $\tilde{\lambda}^{V}_{\mathrm{TPB,per}}$ may shift from a higher value to a lower value with the increasing of $\bar{r}_{\mathrm{el}}/\bar{r}_{\mathrm{ed}}$. Fig. 5a and b also shows that a composite electrode with the broader particle size distributions (represented as larger σ'_{ed} and σ'_{el}) may have a larger percolation volume fraction threshold range ($\psi^{\mathrm{t}}_{\mathrm{ed}}\sim(1-\psi^{\mathrm{t}}_{\mathrm{el}})$). For example, as the non-dimensional standard deviations increase from $\sigma'_{\mathrm{ed}}=\sigma'_{\mathrm{el}}=0$ to $\sigma'_{\mathrm{ed}}=\sigma'_{\mathrm{el}}=0.4$, the range of $\psi^{\mathrm{t}}_{\mathrm{ed}}\sim(1-\psi^{\mathrm{t}}_{\mathrm{el}})$ at $\bar{r}_{\mathrm{el}}/\bar{r}_{\mathrm{ed}}=0.5,\ 1,\ 2,\ 4$ may vary from (0.46–0.82), (0.30–0.70), (0.18–0.54), (0.10–0.37) to (0.32–0.89), (0.20–0.80), (0.11–0.68), (0.06–0.51), respectively. And the maximum $\tilde{\lambda}^{V}_{\mathrm{TPB,per}}$ with $\sigma'_{\mathrm{ed}}=\sigma'_{\mathrm{el}}=0.4$ are 25%, 32%, 25% and 25% lower than the composite electrode with mono particle size distributions ($\sigma'_{\mathrm{ed}}=\sigma'_{\mathrm{el}}=0$) at $\bar{r}_{\mathrm{el}}/\bar{r}_{\mathrm{ed}}=0.5,\ 1,\ 2,\ 4$, respectively.

Although the non-dimensional $\tilde{\lambda}^{V}_{\mathrm{TPB,per}}$ is independent of the practical particle radius, the physical $\lambda^{V}_{\mathrm{TPB,per}}$ actually is determined by many particular microstructure parameters. For example, let $\theta=29.5^{\circ}$ $\phi_g=0.3$, $\psi_{\mathrm{ed}}=0.5$, $\bar{r}_{\mathrm{ed}}=\bar{r}_{\mathrm{el}}=0.25$ μm and $\sigma'_{\mathrm{ed}}=\sigma'_{\mathrm{el}}=0.4$, Fig. 5b can be used to calculate $\lambda^{V}_{\mathrm{TPB,per}}=11.6\times10^{12}$ m^{-2}. Therefore, the curves for non-dimensional properties are very general for practical application, and the relevant effective properties can be easily extracted as physical parameters are specified.

Conclusively, a higher $\lambda^{V}_{\mathrm{TPB,per}}$ may be expected for the composite electrode with small mean particle sizes of both electrode- and electrolyte-materials ($\bar{r}_{\mathrm{ed}}$ and $\bar{r}_{\mathrm{el}}$) and narrow particle size distribu-

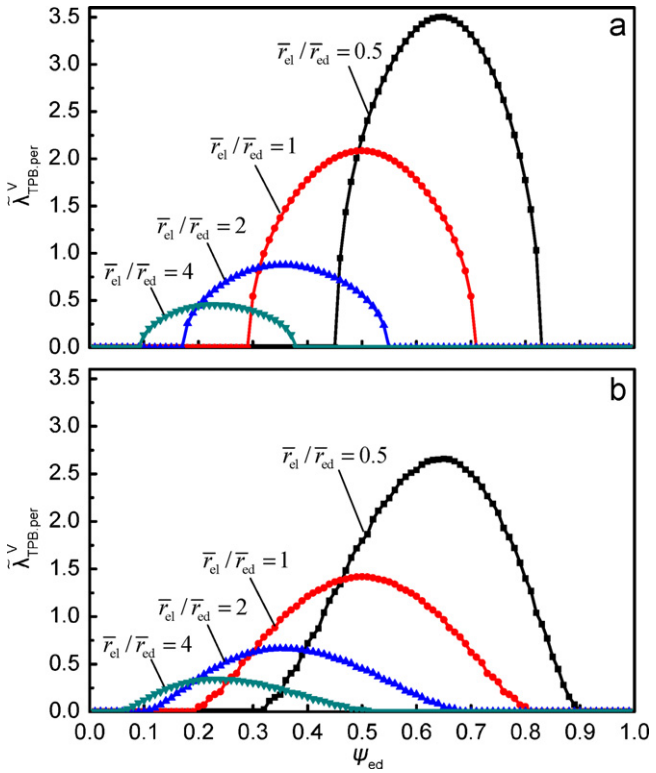

Fig. 5. $\tilde{\lambda}^{V}_{\mathrm{TPB,per}}$ as functions of ψ_{ed} and $\bar{r}_{\mathrm{el}}/\bar{r}_{\mathrm{ed}}$ with (a) $\sigma'_{\mathrm{ed}}=\sigma'_{\mathrm{el}}=0$, (b) $\sigma'_{\mathrm{ed}}=\sigma'_{\mathrm{el}}=0.4$.

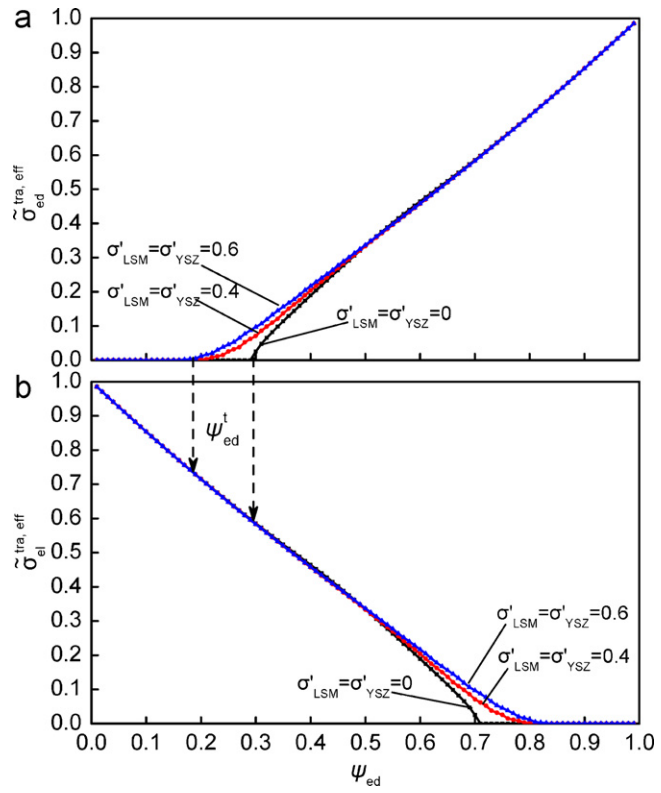

Fig. 6. The non-dimensional effective intra-particle conductivities as functions of ψ_{ed}, σ'_{ed} and σ'_{el} with $\bar{r}_{el}/\bar{r}_{ed}=1$. The upper panel for $\tilde{\sigma}^{tra,eff}_{ed}$ and the lower panel for $\tilde{\sigma}^{tra,eff}_{el}$.

tions (σ'_{ed} and σ'_{el}). And this conclusion may be useful for the SOFC composite cathode (i.e., LSM and YSZ). As there are low exchange transfer current density based on per unit TPB length (low electrochemical activity), a higher $\lambda^{V}_{TPB,per}$ is essential for enhancing the cathode electrochemical performance. Thus, a composite cathode with small mean particle sizes and narrow particle size distributions may lead to the optimized structure.

3.3. Effective intra-particle conductivity

The intra-particle conductivity may become an important parameter for the charge-transfer processes within the composite electrode. In terms of the TPB lengths, there is benefit in representing the results in non-dimensional form. According to Eq. (9), the non-dimensional intra-particle electron conductivity may be written as,

$$\tilde{\sigma}^{tra,eff}_{ed}=\frac{\sigma^{tra,eff}_{ed}}{\sigma^{tra,0}_{ed}(1-\phi_g)^{\mu}}. \quad (18)$$

An analogous definition can also be used for the intra-particle ion conductivity through the electrolyte-particles ($\tilde{\sigma}^{tra,eff}_{el}$).

Fig. 6 illustrates $\tilde{\sigma}^{tra,eff}_{ed}$ and $\tilde{\sigma}^{tra,eff}_{el}$ as functions of the volume fractions of the electrode-material (ψ_{ed}) and non-dimensional standard deviations (σ'_{ed} and σ'_{el}) with $\bar{r}_{el}/\bar{r}_{ed}=1$. As indicated in Fig. 6a, $\tilde{\sigma}^{tra,eff}_{ed}$ may increase with the increasing of ψ_{ed}. And there is also percolation volume fraction threshold limit of the electrode-material (ψ^{t}_{ed}), below which $\tilde{\sigma}^{tra,eff}_{ed}$ is zero.

The present of ψ^{t}_{ed} may be useful for the composite anodes with Ni and YSZ. As there are high electrochemical activity and high specific electron conductivity of Ni ($\sigma^{tra,0}_{ed}$), a higher effective ion conductivity is essential to enhance the ions transfer capability. This in turn may extend the electrochemical active zone and decrease the anodic potential loss. As $\tilde{\sigma}^{tra,eff}_{el}$ may increase with the decreasing of ψ_{ed} (shown in Fig. 6b), the volume fraction of electrode-material (ψ_{ed}) around ψ^{t}_{ed} is always adopted for a composite anode to achieve a high ionic conductivity. In this case, both the electrode- and electrolyte-particles should be percolated and a high effective ionic conductivity can be achieved.

The effects of σ'_{ed} and σ'_{el} on $\tilde{\sigma}^{tra,eff}_{ed}$ and $\tilde{\sigma}^{tra,eff}_{el}$ are also shown in Fig. 6a and b, respectively. It is apparent that there are weak effects of standard deviations on $\tilde{\sigma}^{tra,eff}_{ed}$ and $\tilde{\sigma}^{tra,eff}_{el}$ at a high ψ_{ed}, even with the broad particle size distributions ($\sigma'_{ed}=\sigma'_{el}=0.6$). However, as can be seen from Fig. 6a, the percolation volume fraction threshold of the electrode-material (ψ^{t}_{ed}) may decrease with the increasing of the non-dimensional standard deviations (σ'_{ed} and σ'_{el}). For example, when the non-dimensional standard deviations increase from $\sigma'_{ed}=\sigma'_{el}=0$ to $\sigma'_{ed}=\sigma'_{el}=0.6$, ψ^{t}_{ed} may shift from 0.3 to 0.18. In this case, ψ_{ed} around $\psi^{t}_{ed}=0.18$ (for $\sigma'_{ed}=\sigma'_{el}=0.6$) can be adopted instead of $\psi^{t}_{ed}=0.3$ (for $\sigma'_{ed}=\sigma'_{el}=0$), and a higher $\tilde{\sigma}^{tra,eff}_{el}$ can be achieved. This in turn may increase $\tilde{\sigma}^{tra,eff}_{el}$ from 0.59 to 0.72, approximately.

Analogously, there is also volume fraction threshold limit in Fig. 6b ($1-\psi^{t}_{el}$), above which there is no $\tilde{\sigma}^{tra,eff}_{el}$. And $1-\psi^{t}_{el}$ may shift from 0.7 to 0.82 as the non-dimensional standard deviations increase from $\sigma'_{ed}=\sigma'_{el}=0$ to $\sigma'_{ed}=\sigma'_{el}=0.6$.

Fig. 7 shows $\tilde{\sigma}^{tra,eff}_{ed}$ and $\tilde{\sigma}^{tra,eff}_{el}$ as functions of ψ_{ed} and $\bar{r}_{el}/\bar{r}_{ed}$ with $\sigma'_{ed}=\sigma'_{el}=0.4$. As illustrated in Fig. 7a, for a given ψ_{ed}, $\tilde{\sigma}^{tra,eff}_{ed}$ may increase with the rise of the radial ratio $\bar{r}_{el}/\bar{r}_{ed}$. And $\tilde{\sigma}^{tra,eff}_{el}$, however, may decrease with the increasing of $\bar{r}_{el}/\bar{r}_{ed}$ as shown in Fig. 7b.

For a SOFC composite anode with Ni and YSZ, a volume fraction of the electrode-material (ψ_{ed}) around the percolation volume fraction threshold ψ^{t}_{ed} is always chosen to achieve a high intra-particle

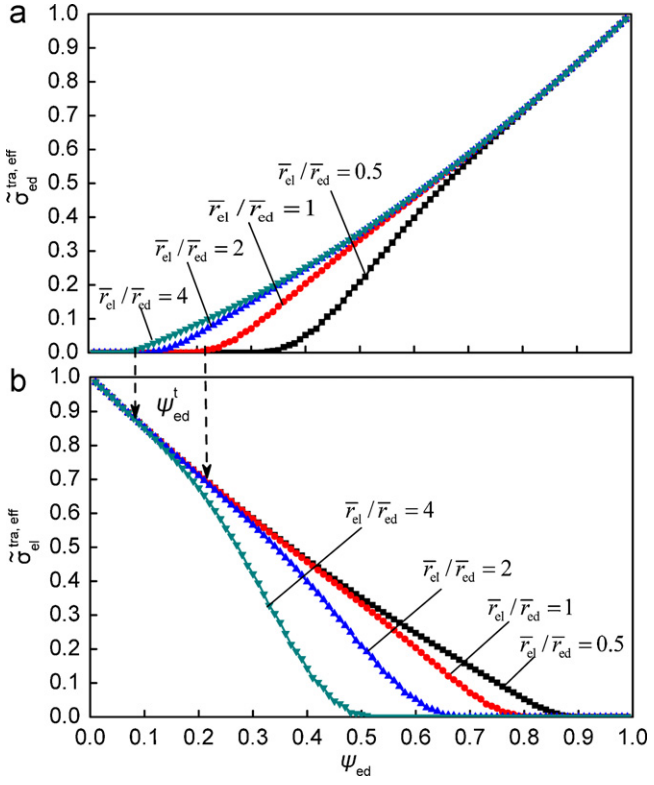

Fig. 7. The non-dimensional effective intra-particle conductivities as functions of ψ_{ed} and $\bar{r}_{el}/\bar{r}_{ed}$ with $\sigma'_{ed}=\sigma'_{el}=0.4$. The upper panel for $\tilde{\sigma}^{tra,eff}_{ed}$ and the lower panel for $\tilde{\sigma}^{tra,eff}_{el}$.

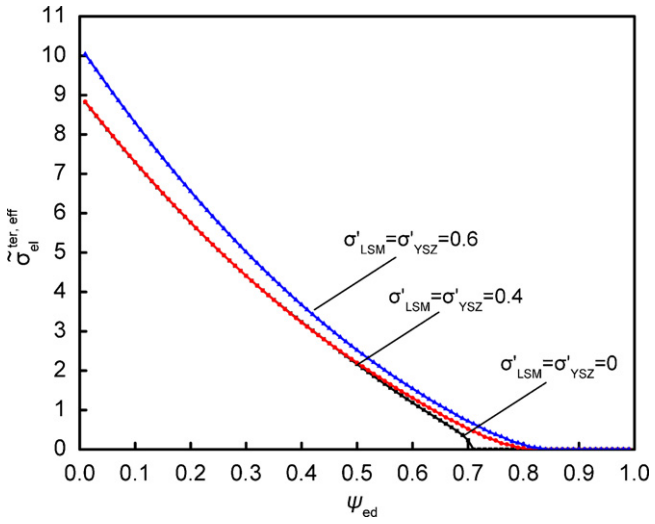

Fig. 8. The non-dimensional inter-particle ion conductivity as a function of ψ_{ed}, σ'_{ed} and σ'_{el} with $\bar{r}_{el}/\bar{r}_{ed} = 1$.

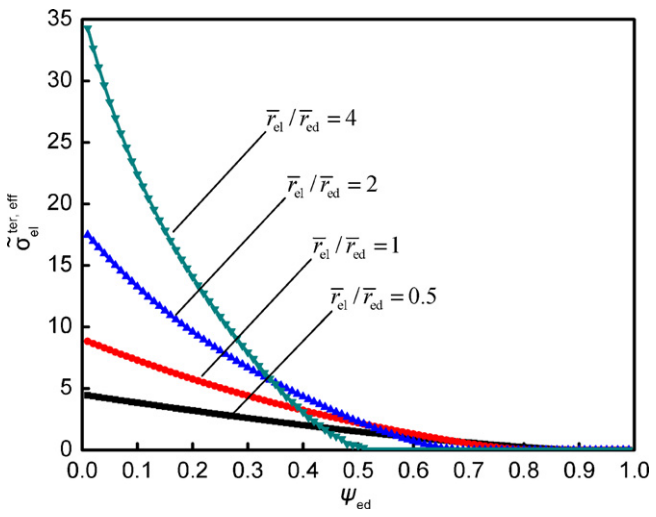

Fig. 9. The non-dimensional inter-particle ion conductivity as functions of ψ_{ed} and $\bar{r}_{el}/\bar{r}_{ed}$ with $\sigma'_{ed} = \sigma'_{el} = 0.4$.

ion conductivity. Although $\tilde{\sigma}_{el}^{tra,eff}$ may decrease with the rise of $\bar{r}_{el}/\bar{r}_{ed}$ at a given ψ_{ed} (shown in Fig. 7b), ψ_{ed}^{t} may also decrease with the increasing of $\bar{r}_{el}/\bar{r}_{ed}$ (shown in Fig. 7a). Therefore, a high $\tilde{\sigma}_{el}^{tra,eff}$ can still benefit from a large $\bar{r}_{el}/\bar{r}_{ed}$, because of the decreasing of ψ_{ed}^{t}. As shown in Fig. 7a, when $\bar{r}_{el}/\bar{r}_{ed}$ increase from 1 to 4, a higher $\tilde{\sigma}_{el}^{tra,eff}$ can be obtained by using a ψ_{ed} around $\psi_{ed}^{t} = 0.1$ (for $\bar{r}_{el}/\bar{r}_{ed} = 4$) instead of $\psi_{ed}^{t} = 0.22$ (for $\bar{r}_{el}/\bar{r}_{ed} = 1$). Under the circumstances, $\tilde{\sigma}_{el}^{tra,eff}$ may increases from 0.7 to 0.88, approximately (shown in Fig. 7b).

Based upon the earlier literature, Chan et al. [21] reported that the specific intra-particle electron and ion conductivities for LSM and YSZ are around $\sigma_{ed}^{tra,0} = 10,000$ S m^{-1} (specific resistivity around 0.0001 Ω m) and $\sigma_{el}^{tra,0} = 6.7$ S m^{-1} (specific resistivity around 0.15 Ω m) at 945 °C, respectively. Considering a situation where $\phi_g = 0.3$, $\psi_{ed} = 0.5$, $\bar{r}_{ed}/\bar{r}_{el} = 1$ μm and $\sigma'_{ed} = \sigma'_{el} = 0.4$, the effective intra-particle electron and ion conductivities can be evaluated as $\sigma_{ed}^{tra,eff} = 1953$ S m^{-1} and $\sigma_{el}^{tra,eff} = 1.3$ S m^{-1} through Fig. 7a and b, respectively.

3.4. Effective inter-particle conductivity

Fig. 8 shows the non-dimensional inter-particle ion conductivity ($\tilde{\sigma}_{el}^{ter,eff}$) as a function of ψ_{ed}, σ'_{ed} and σ'_{el} with $\bar{r}_{ed}/\bar{r}_{el} = 1$. $\tilde{\sigma}_{el}^{ter,eff}$ is defined as,

$$\tilde{\sigma}_{el}^{ter,eff} = \frac{\sigma_{el}^{ter,eff}}{\sigma_{el}^{ter,0}\bar{r}_{ed}\sin^2\theta(1-\phi_g)/\delta}. \quad (19)$$

For YSZ, the inter-particle thicknesses δ have been estimated to be around 5 nm [39].

As illustrated in Fig. 8, $\tilde{\sigma}_{el}^{ter,eff}$ may decrease with the increasing of the volume fraction of electrode-material (ψ_{ed}) with $\bar{r}_{ed}/\bar{r}_{el} = 1$. For the narrow particle size distributions (i.e., $\sigma'_{ed} = \sigma'_{el} \leq 0.4$), there are weak effects of the non-dimensional standard deviations on $\tilde{\sigma}_{el}^{ter,eff}$. For the broad particle size distributions (i.e., $\sigma'_{ed} = \sigma'_{el} = 0.6$), however, the effects of non-dimensional standard deviations on $\tilde{\sigma}_{el}^{ter,eff}$ may not be ignored in practice. And there exist about approximate 10% increase compared to the composite electrode with mono particle size distributions ($\sigma'_{ed} = \sigma'_{el} = 0$).

Fig. 9 shows $\tilde{\sigma}_{el}^{ter,eff}$ as functions of ψ_{ed} and $\bar{r}_{el}/\bar{r}_{ed}$ with $\sigma'_{ed} = \sigma'_{el} = 0.4$. As indicated in Fig. 9, $\tilde{\sigma}_{el}^{ter,eff}$ may increase with the rise of $\bar{r}_{el}/\bar{r}_{ed}$ for a given ψ_{ed}. Furthermore, although the function form of the non-dimensional $\tilde{\sigma}_{el}^{ter,eff}$ is independent of the particular particle radii, the physical inter-particle ion conductivity $\sigma_{el}^{ter,eff}$ is proportional to the mean particle size of each material. And the physical $\sigma_{el}^{ter,eff}$ may significantly increase with the rise of the mean particle size of the electrolyte-material ($\bar{r}_{el}$).

Chan et al. [21] also reported that the specific inter-particle ion conductivity for YSZ is around $\sigma_{el}^{ter,0} = 0.05$ S m^{-1} at 945 °C (i.e., specific resistivity around 20 Ω m). Consider an example of $\theta = 29.5°$ $\phi_g = 0.3$, $\psi_{ed} = 0.5$, $\bar{r}_{ed} = \bar{r}_{el} = 0.25$ μm and $\sigma'_{ed} = \sigma'_{el} = 0.4$, the inter-particle ion conductivity can be evaluated as $\sigma_{el}^{ter,eff} = 0.87$ S m^{-1} by Fig. 9. Thus $\sigma_{el}^{ter,eff} = 0.87$ S m^{-1} has the same order of magnitude with the intra-particle ion conductivity ($\sigma_{el}^{tra,eff} = 1.3$ S m^{-1}), which illustrates that the inter-particle ion conductivity of YSZ can play an important role on overall ionic conductivity.

In conclusion, although the large $\bar{r}_{el}/\bar{r}_{ed}$ and non-dimensional standard deviations may lead to a low $\lambda_{TPB,per}^{V}$, they are helpful for achieving a high effective ionic conductivity. A composite electrode with a large $\bar{r}_{el}/\bar{r}_{ed}$ and broad particle size distributions can not only provide the higher $\sigma_{el}^{ter,eff}$, but also reduce the percolation volume fraction threshold of electrode-material (ψ_{ed}^{t}). As a composite anode is of the high electrochemical activity and intrinsic electronic conductivity, ψ_{ed} around ψ_{ed}^{t} is usually used to achieve the higher intra-particle ion conductivity. Therefore, both $\sigma_{el}^{tra,eff}$ and $\sigma_{el}^{ter,eff}$ may benefit from large $\bar{r}_{el}/\bar{r}_{ed}$, σ'_{ed} and σ'_{el}, due to the increase of $\sigma_{el}^{ter,eff}$ and reduction of ψ_{ed}^{t}. Furthermore, the results are consistent to Itoh et al. and Kim et al. finding that the composite anode using larger mean particle radius of electrolyte-material and broad particle size distribution may effectively prevent the agglomeration of Ni particles and increase the durability of the SOFC during long-term running [40,41].

4. Summary and conclusions

A percolation micro-model has been developed to predict the effective properties of a SOFC composite electrode with polydisperse particles. The properties include the intra/inter-particle ion conductivities ($\sigma_{el}^{tra,eff}$ and $\sigma_{el}^{ter,eff}$), percolated TPB lengths per unit volume ($\lambda_{TPB,per}^{V}$), percolated TPB lengths per dense electrolyte surface ($\lambda_{TPB,per}^{S}$) and hydraulic pore radius (r_g). These properties depend upon the physical characteristics of the microstructure, such as the mean particle sizes of the electrode- and electrolyte-

materials ($\bar{r}_{ed}$ and $\bar{r}_{el}$), volume fraction of the electrode-material (ψ_{ed}), non-dimensional standard deviation of each material phase (σ'_{ed} and σ'_{el}), intrinsic material properties and the porosity (ϕ_g). And the proposed percolation micro-model can be conveniently incorporated with the cell-level model for optimization of the composite electrode structure.

The percolation micro-model has been validated through comparing with the simulated results by the random packing reconstruction method [20], which demonstrates the accuracy of the percolation micro-model in dealing with the composite electrode with poly-disperse particle size distributions.

The results showed that a higher $\lambda^{V}_{TPB,per}$ may be expected for the composite electrode with small mean particle sizes of the electrode- and electrolyte-materials ($\bar{r}_{ed}$ and $\bar{r}_{el}$) and narrow particle size distributions. And a composite cathode with LSM and YSZ may benefit from it for pursuing a high SOFC performance.

The results also indicated that a composite anode with large $\bar{r}_{el}/\bar{r}_{ed}$ and broad particle size distributions can not only prevent the agglomeration of the Ni particles, but also increase the inter-particle ion conductivity and reduce the percolation volume fraction threshold of the electrode-material (ψ^{t}_{ed}). And this conclusion may be useful for a composite anode with Ni and YSZ to achieve a high overall ionic conductivity.

Acknowledgements

This work was supported by Jiangsu University of Science and Technology via a grant (35011005). The authors gratefully acknowledge Prof. Zijing Lin (University of Science and Technology of China) and Prof. Robert J. Kee (Colorado School of Mines) for insightful discussions on the application of percolation theory in SOFCs. We thank the anonymous reviewers whose comments lead to an improved manuscript.

References

[1] J. Deseure, Y. Bultel, L. Dessemond, E. Siebert, Electrochim. Acta 50 (10) (2005) 2037–2046.
[2] X.J. Chen, S.H. Chan, K.A. Khor, Electrochim. Acta 49 (11) (2004) 1851–1861.
[3] N.P. Brandon, D.J. Brett, Philos. Trans. R. Soc. A: Math. Phys. Eng. Sci. 364 (1838) (2006) 147–159.
[4] D. Chen, W. Bi, W. Kong, Z. Lin, J. Power Sources 195 (2010) 6598–6610.
[5] F. Zhao, A.V. Virkar, J. Power Sources 141 (1) (2005) 79–95.
[6] J.H. Yu, G.W. Park, S. Lee, S.K. Woo, J. Power Sources 163 (2) (2007) 926–932.
[7] D.H. Jeon, J.H. Nam, C.J. Kim, J. Electrochem. Soc. 153 (2) (2006) A406–A417.
[8] M.M. Hussain, X. Li, I. Dincer, Int. J. Hydrogen Energy 34 (7) (2009) 3134–3144.
[9] D. Chen, Z. Lin, H. Zhu, R.J. Kee, J. Power Sources 191 (2009) 240–252.
[10] H. Iwai, N. Shikazono, T. Matsui, H. Teshima, M. Kishimoto, R. Kishida, D. Hayashi, K. Matsuzaki, D. Kanno, M. Saito, H. Muroyama, K. Eguchi, N. Kasagi, H. Yoshida, J. Power Sources 195 (4) (2010) 955–961.
[11] J.R. Wilson, J.S. Cronin, A.T. Duong, S. Rukes, H.Y. Chen, K. Thornton, D.R. Mumm, S. Barnett, J. Power Sources 195 (7) (2010) 1829–1840.
[12] L. Lu, D. Chen, F. Sun, X. Ren, Z. Han, G. Guo, Chem. Phys. Lett. (2010).
[13] L. Lu, X. Xu, W. Liang, H. Lu, J. Phys.: Condens. Matter 19 (2007) 406221.
[14] J.R. Wilson, W. Kobsiriphat, R. Mendoza, H.Y. Chen, J.M. Hiller, D.J. Miller, K. Thornton, P.W. Voorhees, S.B. Adler, S.A. Barnett, Nat. Mater. 5 (7) (2006) 541–544.
[15] R.J. Gorte, J.M. Vohs, Curr. Opin. Colloid Interface Sci. 14 (4) (2009) 236–244.
[16] R.M.C. Clemmer, S.F. Corbin, Solid State Ionics 180 (9–10) (2009) 721–730.
[17] J. Golbert, C.S. Adjiman, N.P. Brandon, Ind. Eng. Chem. Res. 47 (20) (2008) 7693–7699.
[18] L.C.R. Schneider, C.L. Martin, Y. Bultel, L. Dessemond, D. Bouvard, Electrochim. Acta 52 (9) (2007) 3190–3198.
[19] A. Ali, X. Wen, K. Nandakumar, B.J. Luo, K.T. Chuang, J. Power Sources 185 (2) (2008) 961–966.
[20] B. Kenney, M. Valdmanis, C. Baker, J.G. Pharoah, K. Karan, J. Power Sources 189 (2) (2009) 1051–1059.
[21] S.H. Chan, X.J. Chen, K.A. Khor, J. Electrochem. Soc. 151 (1) (2004) A164–A172.
[22] P. Costamagna, P. Costa, V. Antonucci, Electrochim. Acta 43 (3–4) (1998) 375–394.
[23] H. Zhu, R.J. Kee, J. Electrochem. Soc. 155 (7) (2008) B715–B729.
[24] V.M. Janardhanan, V. Heuveline, O. Deutschmann, J. Power Sources 178 (1) (2008) 368–372.
[25] F. Zhao, Z.Y. Wang, M.F. Liu, L. Zhang, C.R. Xia, F.L. Chen, J. Power Sources 185 (1) (2008) 13–18.
[26] J. Yoon, R. Araujo, N. Grunbaum, L. Baque, A. Serquis, A. Caneiro, X.H. Zhang, H.Y. Wang, Appl. Surf. Sci. 254 (1) (2007) 266–269.
[27] H.S. Song, S. Lee, S.H. Hyun, J. Kim, J. Moon, J. Power Sources 187 (1) (2009) 25–31.
[28] J.G.P.R. Shearing, R.J. Chater, N.P. Brandon, Chem. Eng. Sci. 64 (2009) 3928–3933.
[29] N. Yao, Ion Beam System Basics and Applications, University of Cambridge, NY, 2007.
[30] M.G. Politis, E.S. Kikkinides, M.E. Kainourgiakis, A.K. Stubos, Microporous Mesoporous Mater. 110 (1) (2008) 92–99.
[31] M. Suzuki, T. Oshima, Powder Technol. 35 (1983) 159–166.
[32] D. Bouvard, F.F. Lange, Acta Metall. Mater. 39 (12) (1991) 3083–3090.
[33] J.H. Nam, D.H. Jeon, Electrochim. Acta 51 (17) (2006) 3446–3460.
[34] M. Suzuki, T. Oshima, Powder Technol. 44 (1985) 213–218.
[35] X.J. Chen, K.A. Khor, S.H. Chan, L.G. Yu, Mat. Sci. Eng. A-Struct. 335 (1–2) (2002) 246–252.
[36] R. Suwanwarangkul, E. Croiset, E. Entchev, S. Charojrochkul, M.D. Pritzker, M.W. Fowler, P.L. Douglas, S. Chewathanakup, H. Mahaudom, J. Power Sources 161 (1) (2006) 308–322.
[37] R. Suwanwarangkul, E. Croiset, M.W. Fowler, P.L. Douglas, E. Entchev, M.A. Douglas, J. Power Sources 122 (1) (2003) 9–18.
[38] W.X. Bi, D.F. Chen, Z.J. Lin, Int. J. Hydrogen Energy 34 (9) (2009) 3873–3884.
[39] B.J.M.a.A.J.B.M.J. Verkerk, Solid State Ionics 6 (1982) 159–170.
[40] H. Itoh, T. Yamamoto, M. Mori, T. Horita, N. Sakai, H. Yokokawa, M. Dokiya, J. Electrochem. Soc. 144 (2) (1997) 641–646.
[41] S.D. Kim, H. Moon, S.H. Hyun, J. Moon, J. Kim, H.W. Lee, J. Power Sources 163 (1) (2006) 392–397.